

A Wireless Power Transfer System for MRI Scanners

Kelly Byron¹, Fraser Robb², Shreyas Vasanawala¹, John Pauly¹ and Greig Scott¹

¹Stanford University, United States ²GE Healthcare, United States

kbyron@stanford.edu; fraser.robb@ge.com; vasanawala@stanford.edu; pauly@stanford.edu; greig@mrsrl.stanford.edu

Abstract—Wireless power transfer is a key component to creating comfortable and completely wireless MRI receive coil arrays. Here, a WPT system is presented using a Class-E power amplifier driving an array of primary coils with a single secondary coil and Class-E rectifier. An RF MEMs switched adjustable impedance matching system is added to match the variable load presented by the coupled coils to the desired load of the power amplifier. The system is shown to be capable of transferring several watts of power inside the MRI bore.

Index Terms—wireless power transmission, impedance matching, microelectromechanical systems.

I. INTRODUCTION

WIRELESSLY powered medical devices present unique challenges to traditional wireless power transfer (WPT) systems, often restricting power levels and device dimensions while increasing the robustness required for dynamic environments. In Magnetic Resonance Imaging (MRI), there is the added restriction of compatibility with nearby MRI coils and the presence of the large (1.5-3T) magnetic field. MRI coil arrays that detect the nuclear magnetic resonance (NMR) signal from the patient are trending to larger channel counts. These are preferably placed directly on the patient to increase signal-to-noise ratio (SNR), leading to recent efforts to make coil arrays lighter and less rigid for patient comfort. Flexible coils have the added benefit of further improving SNR [1]–[3]. In addition to using lighter, flexible coils, the weight of the array can also be significantly reduced by removing bulky connectors, baluns and external cabling. This has led to the goal of making completely wireless and wearable coil arrays powered by WPT technology. To support 100-300 mW per MRI receive channel, a WPT system must be capable of delivering 3-10 Watts for a 32 channel system. This could be achieved with a flexible WPT secondary coil and rectifier components integrated with wearable receive electronics in conformal MRI coil arrays.

In this paper we present a WPT prototype that can operate inside the MRI bore and only requires DC supply and signal generator lines routed outside the scan room. A Class-E power amplifier drives an array of primary coils with a single secondary coil and Class-E rectifier. A tunable impedance matching system using RF MEMs switches is designed and presented to match the variable load presented by the coupled coils to the desired load of the power amplifier. This allows for a sufficient system efficiency to transfer several watts of power. The system is compatible with the MRI environment and capable of transferring power inside the MRI bore.

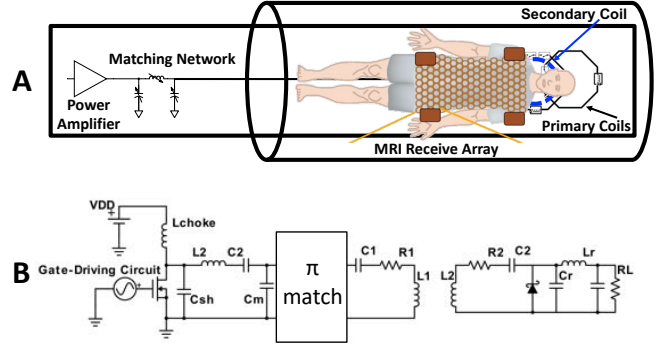


Fig. 1. Wireless power transfer system A: Integrated into the MRI bore and B: Circuit representation with primary side power amplifier and matching network and secondary side diode rectifier and filter.

II. WIRELESS POWER TRANSFER SYSTEM

The concept is to employ an array of WPT drive loops that could be embedded in the MRI patient table, as shown in Figure 1A, to enable variable placement of the secondary loop while maintaining efficient power transfer. Figure 1B shows an equivalent circuit model for the WPT system with an inductively coupled coil pair, modeled as a loosely coupled transformer [4]. The coupled coils present a variable load impedance to the power amplifier dependent on their mutual inductance, which is determined by the geometry and spacing of the coils. The load impedance will change anytime the relative position or distance between the coils is changed. The Class-E power amplifier was chosen for its high efficiency and simple design. However, a major disadvantage of Class-E power amplifiers is their sensitivity to variations in the load impedance. The varying mutual inductance of the coupled coils can result in amplifier efficiency loss and potentially damage the transistor. As a result, we developed a controllable impedance matching system to maintain a reasonable system efficiency over the different stages, as given by:

$$\eta_{system} = \eta_{DC-RF} * \eta_{match} * \eta_{link} * \eta_{RF-DC}. \quad (1)$$

The class E amplifier is based on the EPC9083 demo board which includes the gate driver and eGaN FET. An eGaN device minimizes the parasitic resistance and capacitance [5]. V_{DD} can be varied to provide different power levels to the load, however the parasitic capacitance of the device also varies with V_{DD} , so it is optimized for a V_{DD} of 24 V and P_{out} of 30 W. L_2 and C_2 form an additional filter resonant at the fundamental frequency, with values chosen to provide a Q with the equivalent load resistance that is high enough for the

output voltage to be sinusoidal [6]. L_2 also provides the extra inductance for the power amplifier tuning and is an air-core L_2 of $1.11 \mu\text{H}$ and a non-magnetic RF choke that is $9 \mu\text{H}$ for L_{RFck} . Air-core inductors are essential to avoid saturation in the MRI magnetic field. C_m is used to convert from a 50Ω load to a R_{load} of 9.92Ω for the power amplifier.

Similar to the Class-E power amplifier, a Class-E resonant rectifier is employed to prevent the parasitic capacitance of the diode from de-tuning the coil and to minimize power loss [7]. For an $R_{L,min}$ of 4Ω , L_r is about 200 nH and C_r is about 1.26 nF , which includes the parasitic capacitance of the B540C Schottky diode.

A. Primary Coil Array

Coil-to-coil coupling and link efficiency are maximized when the primary and secondary coils are equal sizes and centered over each other. Since the goal is to integrate the secondary coil with the MRI receive array, it needs to be lightweight and flexible, and is also restricted in size. For example, the secondary could be embedded with the MRI array in a blanket that wraps around the back of the patient while lying on the patient table. This in turn restricts the size of the primary coil for high efficiency, which can lead to difficulty ensuring the coils are aligned in a practical system. As a result, we are using an array of three 20 cm diameter primary coils, shown in Figure 2, that can be switched in individually to maximize coupling to the secondary coil over a large area. The coils are 1 oz copper with tin finish printed on FR-4 .062" material with a trace width of 6.35 mm . Each coil has an inductance of approximately 620 nH and is series-tuned to 10 MHz , which was previously determined to be a good frequency for WPT in the MRI environment [8] to minimize harmonic and noise injection within the MRI frequency band. The primary loops include shielded LC traps at 64 MHz to prevent coupling to the MRI coils. The primary coils have an unloaded Q of about 163 without the MEMS switches. With the addition of the RF MEMS switches, the measured Q of each primary coil drops to about 44 as the result of the approximate 0.5Ω MEMS switch resistances when closed.

To prevent frequency splitting of the resonant loops and eliminate the need for additional switches to detune the coils, adjacent primary coils were overlapped to set their mutual inductance to zero [9]. Two RF MEMS switches are used in series with each coil, one on each side of the coil to fully disconnect common mode cable coupling when the given drive loop is disabled. The MEMS switches control which primary coil transmits power and are described further in Section III-B.

III. TUNABLE IMPEDANCE MATCHING SYSTEM

A. Matching Network Design

Figure 3 shows the tunable pi impedance matching network at the output of the power amplifier. This network switches in binary weighted capacitor and inductor values to adjust for load impedance changes induced on the primary coil. With binary weighted capacitor and inductor values and N switches, 2^N impedances can be matched to the Class E target of 50Ω

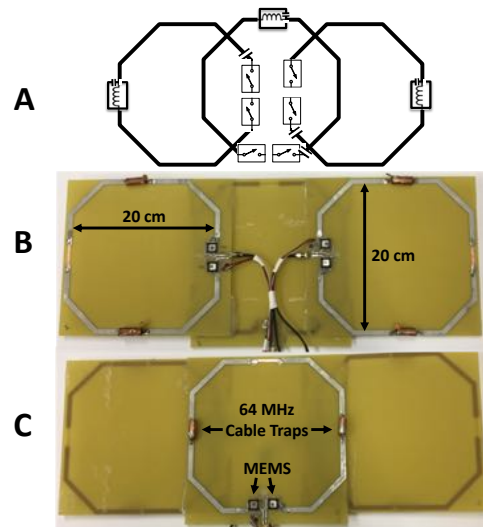


Fig. 2. Array of primary coils A: Schematic with one switch on each side of the series-resonant coils and 64 MHz cable traps on each coil, B: The top of the coils and C: The bottom coil overlapped by the other two coils to decouple the coils at 10 MHz .

Ω . Figure 3B shows that with 12 switches and a C_{min} of 110 pF and L_{min} of 170 nH , we are able to cover almost the entire range of possible reflection coefficients on the Smith chart. Figure 3C shows the efficiency variation of the power amplifier as a manual antenna tuner is used as a simplified load-pull system.

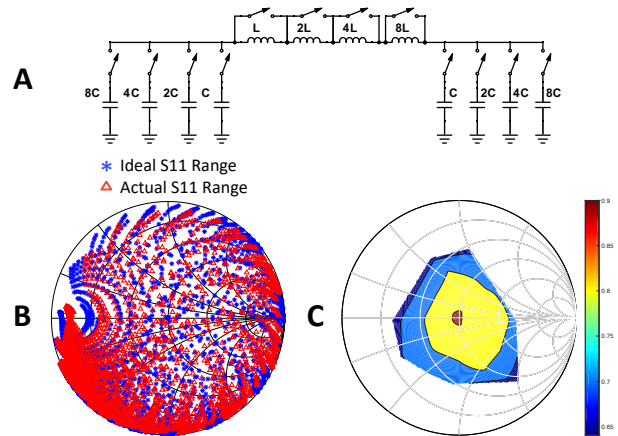


Fig. 3. Impedance matching network A: Circuit with switched capacitors, B: Ideal range of all S11 values and S11 range including switch and board parasitics that can be matched to 50Ω , and C: Efficiency variation of the Class-E power amplifier with simplified load-pull variation.

B. MEMS Switches

The actual switches used in the pi-match circuit must be able to block both positive and negative current and voltage at high power levels. PIN diodes are common in high power applications, however they require RF chokes on each diode that would lead to a bulky design inside the MRI bore [10]. Back-to-back PMOS and NMOS transistors could also be used, but

these have parasitic capacitance values that are relatively large for RF switching. As a result, advanced technology RF MEMS switches were chosen for their low parasitic capacitance and high power capability.

The RF MEMS (General Electric/ MenloMicro M7100) were designed specifically for operation in MRI applications [11] and [12] to reconfigure the geometry of MRI coil arrays or replace the PIN diodes currently used for MR surface coil decoupling. This MEMS switch is non-magnetic for use in the MRI environment, with specified series resistance below 0.5Ω , and can handle high voltage (500 V) and current greater than 5 A .

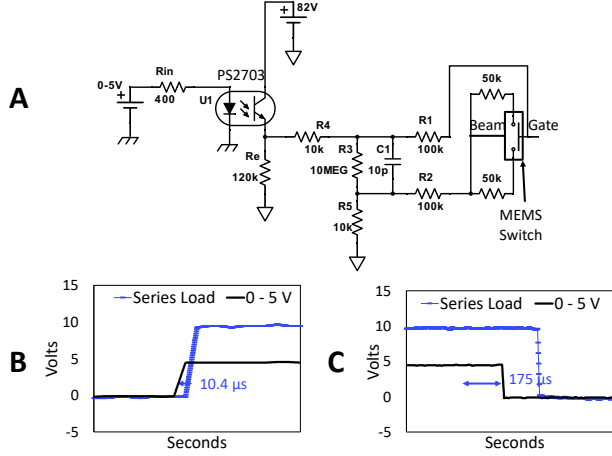


Fig. 4. MEMS gate driver A: Schematic, B: Rise time delay from the 5V signal, and C: Fall time delay from the 5V signal.

The switching speed of the device is limited by the gate driver in our design, shown in Figure 4A. An Arduino microcontroller provides a digital 0-5 V signal to each PS2703 optocoupler to impress the 82 V MEMS gate signal required to close the MEMS switch. The optocoupler has a significantly longer fall time than rise time delay, as shown in Figure 4, which can be shortened by reducing the value of R_e . However, reducing R_e increases the current drawn from the 82 V supply, significantly increasing the power consumption of each switch. With 12 switches being used for the impedance matching network and two switches on each primary coil, we chose a high R_e of $120 \text{ k}\Omega$ to limit power loss, which gave a maximum delay of $175 \mu\text{s}$. Figure 5 shows the populated adjustable pi-matching network PCB, with twelve compact MEMS switches, each with their own gate driver, switching in the binary weighted inductors and capacitors.

C. Additional System Components

The full system diagram with the addition of the switched impedance matching network is shown in Figure 6. To control the impedance matching network, a directional coupler following the power amplifier provides a low power sample of the forward and reflected waves. These signals serve as inputs to an AD8302 gain and phase detector to find the magnitude and phase of the reflection coefficient. The reflection coefficient

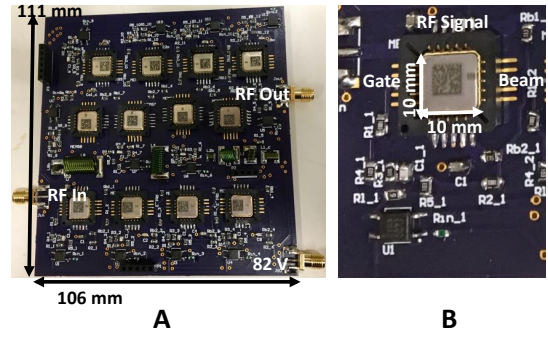


Fig. 5. Adjustable impedance matching board A: With twelve MEMS switches to change the capacitance and inductance of the pi-match and B: Close up of one MEMS switch and gate driver components.

computation is mapped by an Arduino Mega to select the optimal switch combination to match the power amplifier output to 50Ω .

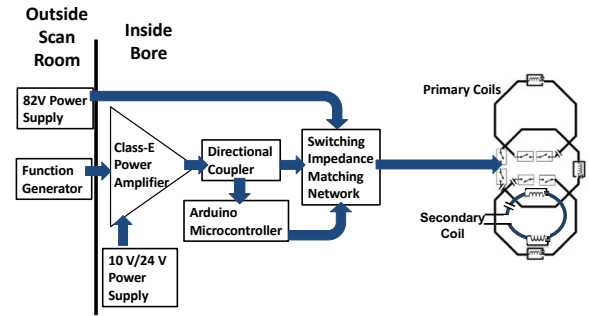


Fig. 6. Full system diagram with the Class-EF power amplifier and switched capacitor matching network. The impedance mismatch is measured by a directional coupler and a gain and phase detector, then an Arduino microcontroller is used to determine and switch in the optimal capacitor values.

A lookup table of all possible reflection coefficients that can be matched to 50Ω for the available inductance and capacitance values is stored on a SD card, connected to the Arduino Mega through an Arduino Ethernet shield. The measured reflection coefficient is compared to the lookup table of reflection coefficients to find the closest match. To account for errors in the phase measurement from the AD8302, the tuning algorithm then sweeps through all switch combinations within 20% of the closest match and with matching network efficiency above 80% and selects the switch combination that gives the lowest measured reflection coefficient magnitude.

IV. RESULTS

Efficiency was measured through each progressive stage of the WPT system at both low and high input DC power levels. The η_{DC-RF} efficiency of the power amplifier was measured with a 50Ω resistor load, showing increasing efficiency with increasing input power levels. This is due to the parasitic capacitance of the transistor decreasing at higher voltages, bringing it closer to the ideal value for the Class-E amplifier. As a result, the efficiency when the power amplifier is connected to the impedance matching system with a 50Ω resistor

TABLE I
MEASURED SYSTEM EFFICIENCY

	Low Input Power	Efficiency	High Input Power	Efficiency
η_{DC-RF}	1.084 W	84.77%	25.704 W	94.98%
$\eta_{DC-RF} * \eta_{match}$	1.142 W	77.86%	22.15 W	86.42%
$\eta_{DC-RF} * \eta_{match} * \eta_{link}$	W	%	W	%
η_{system}	1.478 W	43.68%	21.564 W	62.97%

load also increases at higher input power. Different resistor values (between 15 Ω to 40 Ω) connected to the impedance matching network gave similar efficiencies after tuning. An 18 cm diameter series-resonant secondary coil made of 18 AWG wire with 64 MHz cable traps was used for efficiency measurements. When the secondary coil was 3.5 cm above a primary coil and connected to a 4 Ω resistor load there is again increasing efficiency with increasing input power. Adding the rectifier to measure the efficiency of the complete system gives a final η_{system} of 62.97% while delivering 13.58 W to a 4 Ω resistor load with a 3.5 cm separation between coils.

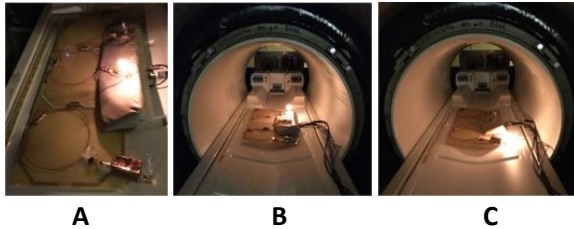


Fig. 7. Individual coils in the primary coil array powering individual secondary coils connected to 7 W lightbulbs in the MRI bore when A: The middle coil is switched on, B: The far coil is switched in, and C: The near coil is switched in.

Figure 7 shows each coil in the WPT primary coil array being switched in individually and coupled to a nearby secondary coil, powering on a lightbulb. This was done inside a 1.5T MRI bore and demonstrates several watts of power being steered and transferred to three separate secondary coils with negligible coupling to the adjacent secondary coils. Further testing is required to determine noise, and add RF gating for active MRI scanning, similar to our first prototype [8].

V. CONCLUSION

This paper presents a complete WPT prototype designed to deliver several watts of power inside the MRI environment with the goal of developing completely wireless MRI patient coils. An array of primary coils that can be individually switched in to steer the power transfer is shown to allow a wide range of secondary coil placements with minimal interactions in the MRI bore. An automated tunable impedance matching network has been designed to provide a constant load to the power amplifier from the varying load of the coupled coils. Both the matching network and array coil switching are performed by non-magnetic high-power RF MEMS switches. Future development will include RF gating and noise assessment to verify that our system has minimal

impact on the MRI image quality. The confined volume of the MRI bore and its unique constraints appear well suited for adaptation of WPT technology.

ACKNOWLEDGMENT

We would like to thank GE Healthcare for their research support, and the assistance of Thomas Grafendorfer. This project is supported by NIH grant R01EB019241.

REFERENCES

- [1] C. J. Hardy, R. O. Giaquinto, J. E. Piel, A. Rohling, W. Kenneth, L. Marinelli, D. J. Blezek, E. W. Fiveland, R. D. Darrow, and T. K. Foo, "128-channel body mri with a flexible high-density receiver-coil array," *Journal of Magnetic Resonance Imaging*, vol. 28, no. 5, pp. 1219–1225, 2008.
- [2] J. R. Corea, P. B. Lechene, M. Lustig, and A. C. Arias, "Materials and methods for higher performance screen-printed flexible mri receive coils," *Magnetic Resonance in Medicine*, 2016.
- [3] S. S. Vasawala, R. Stormont, S. Lindsay, T. Grafendorfer, J. Y. Cheng, J. M. Pauly, G. Scott, J. X. Guzman, V. Taracila, D. Chirayath *et al.*, "Development and clinical implementation of next generation very light weight and extremely flexible receiver arrays for pediatric mri," *arXiv preprint arXiv:1705.00224*, 2017.
- [4] B. Lenaerts and R. Puers, "Inductive link design," *Omnidirectional Inductive Powering for Biomedical Implants*, pp. 39–81, 2009.
- [5] M. de Rooij, "Performance comparison for a4wp class-3 wireless power compliance between egan fet and mosfet in a zvs class d amplifier," in *PCIM Europe 2015; International Exhibition and Conference for Power Electronics, Intelligent Motion, Renewable Energy and Energy Management; Proceedings of VDE*, 2015, pp. 1–8.
- [6] N. O. Sokal, "Class-e rf power amplifiers," *QEX*, vol. 204, pp. 9–20, 2001.
- [7] M. K. Kazimierczuk, "Analysis of class e zero-voltage-switching rectifier," *IEEE transactions on circuits and systems*, vol. 37, no. 6, pp. 747–755, 1990.
- [8] K. Byron, F. Robb, P. Stang, S. Vasawala, J. Pauly, and G. Scott, "An rf-gated wireless power transfer system for wireless mri receive arrays," *Concepts in Magnetic Resonance Part B: Magnetic Resonance Engineering*, pp. e21360–n/a, e21360. [Online]. Available: <http://dx.doi.org/10.1002/cmr.b.21360>
- [9] P. B. Roemer, W. A. Edelstein, C. E. Hayes, S. P. Souza, and O. Mueller, "The nmr phased array," *Magnetic resonance in medicine*, vol. 16, no. 2, pp. 192–225, 1990.
- [10] J. De Mingo, A. Valdovinos, A. Crespo, D. Navarro, and P. Garcia, "An rf electronically controlled impedance tuning network design and its application to an antenna input impedance automatic matching system," *IEEE Transactions on Microwave Theory and Techniques*, vol. 52, no. 2, pp. 489–497, 2004.
- [11] S. Bulumulla, K. Park, E. Fiveland, J. Iannotti, and F. Robb, "Mems switch integrated radio frequency coils and arrays for magnetic resonance imaging," *Review of Scientific Instruments*, vol. 88, no. 2, p. 025003, 2017.
- [12] D. Spence and M. Aimi, "Custom mems switch for mr surface coil decoupling," in *Proc. Int. Soc. Magn. Reson. Med.*, vol. 23, 2015, p. 704.